Single-photon scattering in giant-atom waveguide systems with chiral coupling

Shu-Yu Li,[1] Ze-Quan Zhang,[1] Lei Du,[2] Yong Li,[3,*] and Huaizhi Wu[1,†]

[1]*Fujian Key Laboratory of Quantum Information and Quantum Optics & Department of Physics, Fuzhou University, Fuzhou 350116, People's Republic of China*

[2]*School of Physics and Center for Quantum Sciences, Northeast Normal University, Changchun 130024, China*

[3]*Center for Theoretical Physics & School of Physics and Optoelectronic Engineering, Hainan University, Haikou 570228, China*

(Received 3 January 2024; accepted 14 May 2024; published 5 June 2024)

We study single-photon scattering spectra of a giant atom chirally coupled to a one-dimensional waveguide at multiple connection points, and examine chirality-induced effects in the scattering spectra. We show that the transmission spectra typically possess an anti-Lorentzian lineshape with a nonzero minimum, but by engineering the chirality of the multipoint coupling, the transmission spectrum of an incident photon can undergo a transition from complete transmission to total reflection at multiple frequency "windows," where the width of the anti-Lorentzian lineshape for each of the window can be flexibly tuned at a fixed frequency detuning. Moreover, we show that a perfect nonreciprocal photon scattering can be achieved due to the interplay between internal atomic spontaneous emission and the chirally external decay to the waveguide, in contrast to that induced by the non-Markovian retardation effect. We also consider the non-Markovian retardation effect on the scattering spectra, which allows for a photonic band gap even with only two chiral coupling points. The giant-atom-waveguide system with chiral coupling is a promising candidate for realizing single-photon routers with multiple channels.

DOI: 10.1103/PhysRevA.109.063703

I. INTRODUCTION

Waveguide quantum electrodynamics (QED) [1–3], which studies the interaction between atoms (or other quantum emitters) and free propagating photons in a one-dimensional (1D) waveguide, has been experimentally demonstrated in many state-of-the-art architectures, such as trapped natural or artificial atoms (including quantum dots [4–7], diamond defects [8–11], superconducting qubits [12], and single organic molecules [13]) coupled with optical fibers [14–16], photonic crystal waveguides [17–19], or microwave transmission lines (TLs) [20–24]. Typically, the (natural) atoms are orders of magnitude smaller than optical (microwave) wavelengths of the continuous bosonic modes in the 1D waveguide, therefore, they can be viewed as point-like emitters to justify the dipole approximation. Waveguide QED systems with natural "small" atoms can potentially be used to construct the quantum network [25–27] and simulate quantum many-body physics [28–30]. However, extending the small atom platform to artificial " giant" atomic systems has attracted significant recent attention (see the first review by Kockum [31]), in part, because it represents a breakdown of the dipole approximation where the scale of atoms becomes comparable to the wavelength of the light they interact with. The artificial giant atoms have been well designed and recently demonstrated with superconducting qubits coupled to short-wavelength surface acoustic waves (SAWs) [32–37] or a microwave-waveguide at multiple discrete points [38–40]. The multiple coupling points give rise to self-interference effects, which are quite different from the conventional interference effects among point-like small atoms (or resonators) coupled locally to a common bath. The self-interference effects, which depend on both the distances between coupling points and the photonic frequency, allows to observe several unconventional phenomena, including frequency-dependent Lamb shift and relaxation rate [38,41], decoherence-free atomic states [39,42–45], non-Markovian decay dynamics [34,35,46–48], and chiral light-matter interactions [29,49–53].

A waveguide QED system with giant atoms has emerged as a new promising platform for engineering the transport of photons and single-photon routing [41,49,50,53–61]. The system enables strong tunable atom-waveguide coupling and the engineering of time delay, manifesting multiple-point interference and non-Markovian retardation effects in the photon scattering spectra [50,53,55,56,60]. Herein, the photon scattering spectra can exhibit interesting features, such as electromagnetically induced transparency [57,58,61], atomic decay induced nonreciprocity [50,53,55], and photonic band gap [56,58], and these features can be applied to probe collective radiance and topological states [49,57,58] with a chain of two-level giant atoms in both the Markovian and non-Markovian regimes [41]. Moreover, an experimental setup with chiral interfaces between giant atoms and waveguides has recently become a reality based on technological progress, e.g., by coupling transmon qubits [62,63] to meandering TLs with circulators [64–67]. In these setups, the coupling between waveguide modes and giant atoms depends on the propagation direction of the light. Despite the chirality of their coupling, one can still observe perfect collective radiance and decoherence-free dark states [49] inaccessible with small atoms, and

*Corresponding author: yongli@hainanu.edu.cn
†Corresponding author: huaizhi.wu@fzu.edu.cn

 ©2024 American Physical Society

furthermore, non-Markovianity induced nonreciprocity [50,53] and photon frequency conversion [50], whereas the previous studies about single-photon routing were limited to special cases, e.g., a (multilevel) giant atom with two asymmetric coupling points [50,54]. Thus, it is unclear what can bring about by engineering the chirality with more than two coupling points.

In this paper, we study single-photon scattering spectra and their nonreciprocity with a two-level giant atom chirally coupled to a waveguide at multiple points. We assume equally spaced coupling points, and focus on chirality induced effects by considering three chiral coupling regimes: (1) bidirectional even coupling (BEC); (2) unidirectional uneven coupling (UUEC); and (3) bidirectional uneven coupling (BUEC), respectively. By engineering the chirality of the couplings, we find that an incident photon, which is fully transmitted in the BEC (UUEC) regimes, can become totally reflected in the BUEC regime for a fixed two-point propagating phase. This feature cannot be observed in the nonchiral setting simply by increasing the number of coupling points N [56]. Moreover, the transmission spectra can exhibit multiple $(N-1)$ total reflection "windows" at fixed frequencies whose widths can be flexibly controlled. In comparison, other chiral setups proposed for photon routing are involved with a three-level giant atom [50] or giant-atom pairs (i.e., giant molecules) [53,60] and are limited to the case of two coupling points, preventing it from multiple-window photon routing. We examine the phases of the transmission and reflection coefficients, and find that the giant atom imprints direction-dependent phases on the incident photon uniquely for the chiral setup with uneven couplings.

Furthermore, by taking atomic spontaneous decay into account, we find that a perfect nonreciprocal photon scattering (with transmission probability of unity in the forward direction and zero in the backward), which is inaccessible in the giant-atom-waveguide system with uniformly symmetric coupling [56], can now be realized by engineering the chirality of the atom-waveguide interaction. This is in contrast to other schemes concerning nonreciprocal photon scattering [50,53], where the nonreciprocity is typically induced by non-Markovian retardation effects [53] or by synthetic gauge fields [55]. We also consider the non-Markovian retardation effect on the scattering spectra. We observe a photonic band gap for the spectra in the intermediate non-Markovian regime even with only two chiral coupling points, which normally arises in a setup with a large number of coupling point and with uniformly symmetric coupling [56]. The giant-atom-waveguide system with chiral coupling provides a promising platform for realizing single-photon routers with multiple frequency channels.

The paper is organized as follows. Section II introduces the theoretical model and calculates the transmission and reflection coefficients of an incident photon by using a real-space scattering method, where the giant atom's Lamb shifts and effective decay rates are derived and discussed. Section III presents the scattering spectra for three chiral coupling conditions (i.e., the BEC, the UUEC, and the BUEC conditions) in the Markovian regime and discusses intriguing features induced by the chiral coupling. Section IV shows that nonreciprocal photon scattering can be realized due to the cooperative effect of chiral coupling and atomic spontaneous decay. Section V further discusses the scattering spectra in the non-Markovian regime, with a conclusion given in Sec. VI.

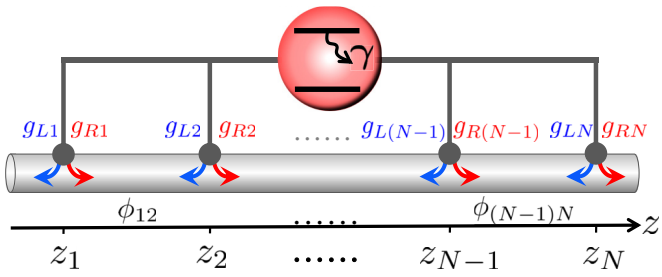

FIG. 1. Schematics of a giant-atom system. A two-level giant atom (with excited state $|e\rangle$ and ground state $|g\rangle$) couples to the one-dimensional waveguide at multiple points (labeled by the coordinates z_j), where g_{Lj} (g_{Rj}) are coupling strengths at the jth coupling point for left-going (right-going) waveguide modes, ϕ_{ij} are distance-dependent phases for the photon propagating between the ith and the jth coupling points, and γ is the spontaneous decay rate of the atom to the bath environment.

II. MODEL AND METHOD

As schematically shown in Fig. 1, the system consists of a two-level giant atom chirally coupled to a 1D waveguide at N discrete points (labeled j, coordinates z_j). The coupling strengths between the giant atom and waveguide modes depend on the propagation direction of the light. Under the rotating-wave approximation, the total Hamiltonian of the system in real space can be written as ($\hbar = 1$ hereafter) [68]

$$H = H_a + H_w + H_{\rm int}, \tag{1}$$

with

$$\begin{aligned} H_a &= (\omega_e - i\gamma)|e\rangle\langle e|, \\ H_w &= \int_{-\infty}^{+\infty} dz a_L^\dagger(z)\left(\omega_0 + iv_g\frac{\partial}{\partial z}\right)a_L(z) \\ &\quad + a_R^\dagger(z)\left(\omega_0 - iv_g\frac{\partial}{\partial z}\right)a_R(z), \\ H_{\rm int} &= \int_{-\infty}^{+\infty} dz\sum_{j=1}^{N}\delta(z-z_j)\sqrt{v_g}[g_{Lj}a_L^\dagger(z)e^{ik_0 z} \\ &\quad + g_{Rj}a_R^\dagger(z)e^{-ik_0 z}]|g\rangle\langle e| + \text{H.c.}, \end{aligned}$$

where H_a is the bare atomic Hamiltonian, with ω_e being the transition frequency between the ground state $|g\rangle$ and the excited state $|e\rangle$, and γ being the spontaneous emission rate induced by the nonwaveguide modes in the environment. H_w is the bare waveguide Hamiltonian, with $a_L^\dagger(z)[a_R^\dagger(z)]$ and $a_L(z)$ $[a_R(z)]$ the creation and annihilation operators of the left-propagating (right-propagating) modes at position z. ω_0 is the central frequency around which a linear dispersion relation under consideration is given by $\omega(k) = \omega_0 + (k-k_0)v_g$ with k the wave vector of the incident photon, k_0 the wave vector corresponding to ω_0, and v_g the group velocity in the vicinity of ω_0 [69]. $H_{\rm int}$ is the interaction Hamiltonian with g_{Lj} and g_{Rj} the renormalized coupling strengths for the atom interacting

with a left-going and right-going photon at the position $z = z_j$, respectively, where in real space, the giant atom behaves as a potential $\delta(z - z_j)$ at each coupling point. Note that the atom-waveguide coupling at multiple points enable us to observe system dynamics in both the Markovian and non-Markovian regimes [49,53], which strongly depends on the accumulated phases $\phi_{ij} = k|z_i - z_j|$ [or $\phi_{ij} = (\omega - \omega_0)\tau_{ij} + k_0|z_i - z_j|$] of photons propagating between any two of the N coupling points with $\tau_{ij} = |z_i - z_j|/v_g$.

We consider the single-photon scattering problem by engineering the chirality of the atom-waveguide couplings, where the system is constrained to the single excitation subspace, and then the eigenstate of Hamiltonian (1) is given by

$$|\psi\rangle = \int_{-\infty}^{+\infty} dz[c_{gL}(z)a_L^\dagger(z) + c_{gR}(z)a_R^\dagger(z)]|g,0\rangle + c_{e0}|e,0\rangle, \tag{2}$$

where $c_{gL}(z)$ [$c_{gR}(z)$] is the probability amplitude of the states $a_L^\dagger(z)|g,0\rangle$ [$a_R^\dagger(z)|g,0\rangle$], describing a left-propagating (right-propagating) photon at position z and the atom in $|g\rangle$, and c_{e0} is the probability amplitude of the atom in the excited state $|e\rangle$, finding no photon in the waveguide.

Solving the stationary Schrödinger equation $H|\psi\rangle = E|\psi\rangle$ with an appropriate ansatz for the probability amplitudes $c_{gL}(z)$ and $c_{gR}(z)$ (see Appendix A), we obtain the transmission and reflection coefficients for a left-incident photon

$$t_N = \frac{(\Delta - \Delta_{ls}) + i(\gamma + \Gamma_L - \Gamma_R)}{(\Delta - \Delta_{ls}) + i(\gamma + \Gamma_L + \Gamma_R)},$$
$$r_1 = \frac{-i\Gamma_{LR}}{(\Delta - \Delta_{ls}) + i(\gamma + \Gamma_L + \Gamma_R)}, \tag{3}$$

and for a right-incident photon

$$\tilde{t}_1 = \frac{(\Delta - \Delta_{ls}) + i(\gamma - \Gamma_L + \Gamma_R)}{(\Delta - \Delta_{ls}) + i(\gamma + \Gamma_L + \Gamma_R)},$$
$$\tilde{r}_N = \frac{i\Gamma_{LR}^*}{(\Delta - \Delta_{ls}) + i(\gamma + \Gamma_L + \Gamma_R)}, \tag{4}$$

where $\Delta = \omega(k) - \omega_e$ is the detuning between the incident photons and the atomic transition $|g\rangle \leftrightarrow |e\rangle$; $\Delta_{ls} \equiv \Delta_L + \Delta_R$ is the overall Lamb shift contributed by both the left- and right-propagating directions' waveguide modes from interference between connection points, with

$$\Delta_L = \frac{1}{2}\sum_{i,j}^{N} g_{Li}g_{Lj}\sin\phi_{ij}, \quad \Delta_R = \frac{1}{2}\sum_{i,j}^{N} g_{Ri}g_{Rj}\sin\phi_{ij}, \tag{5}$$

correspondingly; Γ_L and Γ_R are the direction-dependent relaxation rates given by [38,56]

$$\Gamma_L = \frac{1}{2}\sum_{\{i,j\}=1}^{N} g_{Li}g_{Lj}\cos\phi_{ij}, \tag{6}$$

$$\Gamma_R = \frac{1}{2}\sum_{\{i,j\}=1}^{N} g_{Ri}g_{Rj}\cos\phi_{ij}, \tag{7}$$

and

$$\Gamma_{LR} = \left(\sum_{i=1}^{N} e^{ikz_i}g_{Li}\right)\left(\sum_{j=1}^{N} e^{ikz_j}g_{Rj}\right). \tag{8}$$

It follows that the transmission and reflection probabilities are defined by $\mathcal{T}_L = |t_N|^2$ ($\mathcal{T}_R = |\tilde{t}_1|^2$) and $\mathcal{R}_L = |r_1|^2$ ($\mathcal{R}_R = |\tilde{r}_N|^2$), respectively. Note that the (chiral) atom-photon interaction is imprinted on the phases of the transmission and reflection coefficients, which depend on the Lamb shift Δ_{ls} and the direction-dependent relaxation rates Γ_L and Γ_R. In particular, for $\mathcal{T}_{L(R)} = 1$ or $\mathcal{R}_{L(R)} = 1$, the phase imprinted on the scattering photon can depend on the incident direction and the chirality of couplings, see the further discussion later.

Revisiting the small-atom limit [38], where the atom interacts with the left-going (right-going) waveguide modes by a single connection point (e.g., at position z_j), the atomic relaxation rates into the continuum modes can be simply derived by Fermi's golden rule and are given by $g_{Lj}^2/2$ and $g_{Rj}^2/2$, and the atomic ground state is not shifted by the atom-waveguide coupling (i.e., $\Delta_{L(R)} = 0$) [38]. In the case of a giant-atom with N connection points, when the couplings with left-going and right-going photons are uniformly symmetric, i.e., $g_{Li} = g_{Lj} = g_{Ri} = g_{Rj}$ (for all $i \neq j$), one finds $\Delta_L = \Delta_R$ and $\Gamma_L = \Gamma_R$ regardless of the details of phases ϕ_{ij}, then the transmission and reflection probabilities read

$$\mathcal{T}_L = \mathcal{T}_R = \frac{(\Delta - 2\Delta_L)^2 + \gamma^2}{(\Delta - 2\Delta_L)^2 + (\gamma + 2\Gamma_L)^2}, \tag{9}$$

$$\mathcal{R}_L = \mathcal{R}_R = \frac{4\Gamma_L^2}{(\Delta - 2\Delta_L)^2 + (\gamma + 2\Gamma_L)^2}. \tag{10}$$

For $\gamma = 0$, the reflection probabilities have the standard Lorentzian lineshapes centered at $\Delta = 2\Delta_L$ with the full-width at half-maximum (FWHM) $4\Gamma_L$ and the transmission probabilities have the anti-Lorentzian lineshapes. There exists a singular point with $\Gamma_L = 0$ for which the giant atom decouples from the waveguide, leading to $\mathcal{T}_L = \mathcal{T}_R = 1$. Moreover, Eqs. (9) and (10) imply that nonreciprocal photon scattering cannot happen whether $\gamma = 0$ or $\gamma \neq 0$.

To clearly see chirality induced features, we now consider the N coupling points being equally spaced and first focus on the effect of even or uneven chiral coupling in the Markovian regime, where the propagating time of the photons' travel between the leftmost and the rightmost coupling points $\tau_{1N} = (z_N - z_1)/v_g$ is short compared to the characteristic relaxation time $\sim\tilde{\Gamma}^{-1}$ of the giant atom with $\tilde{\Gamma} = [(\sum_{i=1}^{N} g_{Li})^2 + (\sum_{j=1}^{N} g_{Rj})^2]/2 + \gamma$, corresponding to the decay rate for $\tau_{1N} \to 0$. However, when $\tau_{1N} \sim 1/\tilde{\Gamma}$, the giant atom-waveguide interaction will enter the non-Markovian regime [31,34,38,56], i.e., the time evolution of the system can depend on what the system state was at an earlier time, and will be discussed later in Sec. V. It should be emphasized that the transmission and reflection coefficients in Eqs. (3) and (4) are valid in both the Markovian and the non-Markovian regimes. Moreover, given that the bandwidth Δ is of the order of $\tilde{\Gamma}$, we can examine the Markovian physics based on Eqs. (5)–(7) under the condition of $\tilde{\Gamma}\tau_{1N} \sim |\Delta|\tau_{1N} \ll 1$, and neglect the contribution of $|\Delta|\tau_{1N}$ to the ϕ_{ij}-dependent effect. In the next section, we first replace the phases ϕ_{ij}

by $\tilde{\phi}_{ij} = (\omega_e - \omega_0)\tau_{ij} + k_0|z_i - z_j|$, and the transmission and reflection coefficients are rephrased in terms of the phase difference between adjacent coupling points $\tilde{\phi}_{12}$, i.e., $\phi_{ij} = |j - i|(\Delta\tau_{12} + \tilde{\phi}_{12}) \to \tilde{\phi}_{ij} = |j - i|\tilde{\phi}_{12}$. We take the $\tilde{\phi}_{12}$ modulo 2π [denoted by $\mathrm{mod}(\tilde{\phi}_{12}, 2\pi)$ in the following] into account for its effectiveness, and study photon scattering under different chiral coupling regimes.

III. PHOTON SCATTERING WITH CHIRAL COUPLING: THE MARKOVIAN REGIME

By considering the chiral coupling with $\gamma = 0$ and assuming g_{Li} (g_{Ri}) being positive real values, one typically has $\Gamma_L \neq \Gamma_R$, i.e., $\frac{1}{2}\sum_{\{i,j\}=1}^{N}(g_{Li}g_{Lj} - g_{Ri}g_{Rj})\cos\phi_{ij} \neq 0$. The chirality can be divided into three different regimes: (1) bidirectional even coupling (BEC) $g_{Li} = g_{Lj}, g_{Ri} = g_{Rj}$, but $g_{Li} \neq g_{Ri}$; (2) unidirectional uneven coupling (UUEC) $g_{Li} = g_{Lj}, g_{Ri} \neq g_{Rj}$, or $g_{Li} \neq g_{Lj}, g_{Ri} = g_{Rj}$; and (3) bidirectional uneven coupling (BUEC) $g_{Li} \neq g_{Lj}, g_{Ri} \neq g_{Rj}$. Remarkably, we find that $\Gamma_L = \Gamma_R$ can be achieved by appropriately tuning the uneven coupling strengths distributed at different coupling points. As a result, it offers a flexible way to control the transmission and reflection of a single incident photon and allows for photon routing at multiple fixed frequencies corresponding to $\Delta = \Delta_{ls}$. This will be discussed in detail later.

A. Bidirectional even coupling

We first consider the BEC regime for a giant atom with $N \geqslant 2$ coupling points. The coupling strengths of the N coupling points are identical for the same propagation direction and are set to $g_{Li} = g_L$ and $g_{Ri} = g_R$. Due to the multiple-point interference effect, the overall Lamb shift takes the form

$$\Delta_{ls} = \frac{1}{2}\left(g_L^2 + g_R^2\right)\frac{N\sin\tilde{\phi}_{12} - \sin N\tilde{\phi}_{12}}{1 - \cos\tilde{\phi}_{12}}, \tag{11}$$

and the sum (difference) of the two effective decay rates is given by

$$\Gamma_L \pm \Gamma_R = \frac{1}{2}\left(g_L^2 \pm g_R^2\right)\frac{\sin^2\left(\frac{1}{2}N\tilde{\phi}_{12}\right)}{\sin^2\left(\frac{1}{2}\tilde{\phi}_{12}\right)}, \tag{12}$$

which shows that the photon interferes with itself multiple times independently for the distinct (left and right) propagation directions.

(1) When the two-point propagating phase satisfies $\mathrm{mod}(\tilde{\phi}_{12}, 2\pi) = 0$, the Lamb shift vanishes regardless of the chiral couplings, but the effective decay rates are N^2-enhanced and are given by

$$\Gamma_L \pm \Gamma_R = \tfrac{1}{2}N^2\left(g_L^2 \pm g_R^2\right). \tag{13}$$

The transmission probabilities then read

$$\mathcal{T}_L = \mathcal{T}_R = \frac{4\Delta^2 + N^4\left(g_L^2 - g_R^2\right)^2}{4\Delta^2 + N^4\left(g_L^2 + g_R^2\right)^2}. \tag{14}$$

In contrast to the case with uniformly symmetric coupling ($g_L = g_R$), the chirality of couplings leads to a nonvanishing transmission $\mathcal{T}_{L(R)} \neq 0$ at resonance $\Delta = 0$, i.e.,

$$\mathcal{T}_{L(R)} = \left(\frac{\Gamma_L - \Gamma_R}{\Gamma_L + \Gamma_R}\right)^2 = \left(\frac{g_L^2 - g_R^2}{g_L^2 + g_R^2}\right)^2, \tag{15}$$

corresponding to $\mathcal{T}_{L(R)}$ in the large $N \to \infty$ limit.

(2) For $\mathrm{mod}(\tilde{\phi}_{12}, 2\pi) = 2m'\pi/N$ ($m' = 1, 2, \ldots, N-1$), the Lamb shift can be nonvanishing and is given by

$$\Delta_{ls} = \frac{N}{2}\left(g_L^2 + g_R^2\right)\cot\left(\frac{m'\pi}{N}\right), \tag{16}$$

but the effective decay rates vanish ($\Gamma_L = \Gamma_R = 0$) due to the destructive interference effect among the coupling points. Then, a photon incident from the left or the right will be completely transmitted, independent of the frequency detuning between the incident photon and the atomic transition. This is analogous to the case with uniformly symmetric coupling, except that $\Delta_L \neq \Delta_R$.

B. Unidirectional uneven and bidirectional uneven coupling

The results for the BEC regime can be understood intuitively, but those for the UUEC and the BUEC regime are not self-evident. To obtain instructive insight, we first consider the simplest model with only $N = 2$ coupling points in the Markovian limit, where the Lamb shifts are $\Delta_L = \Delta_R = 0$ both for $\mathrm{mod}(\tilde{\phi}_{12}, 2\pi) = 0$ and $\mathrm{mod}(\tilde{\phi}_{12}, 2\pi) = 2m'\pi/N$, but the sum and difference of the two effective decay rates $\Gamma_L \pm \Gamma_R$ strongly depend on the chirality of the coupling strengths. For $\mathrm{mod}(\tilde{\phi}_{12}, 2\pi) = 0$, the effective decay rates are simply given by

$$\Gamma_L \pm \Gamma_R = \frac{(g_{L1} + g_{L2})^2 \pm (g_{R1} + g_{R2})^2}{2}, \tag{17}$$

and correspondingly the transmission probabilities are

$$\mathcal{T}_{L(R)} = \frac{4\Delta^2 + [(g_{L1} + g_{L2})^2 - (g_{R1} + g_{R2})^2]^2}{4\Delta^2 + [(g_{L1} + g_{L2})^2 + (g_{R1} + g_{R2})^2]^2}; \tag{18}$$

for $\mathrm{mod}(\tilde{\phi}_{12}, 2\pi) = \pi$, the effective decay rates are alternatively given by

$$\Gamma_L \pm \Gamma_R = \frac{(g_{L1} - g_{L2})^2 \pm (g_{R1} - g_{R2})^2}{2}, \tag{19}$$

and the transmission probabilities read

$$\mathcal{T}_{L(R)} = \frac{4\Delta^2 + [(g_{L1} - g_{L2})^2 - (g_{R1} - g_{R2})^2]^2}{4\Delta^2 + [(g_{L1} - g_{L2})^2 + (g_{R1} - g_{R2})^2]^2}. \tag{20}$$

Note that in the UUEC regime [i.e., $g_{L1} = g_{L2}$ and $g_{R1} \neq g_{R2}$ (or $g_{R1} = g_{R2}$ and $g_{L1} \neq g_{L2}$)], if the coupling strengths satisfy $g_{L1} + g_{L2} = g_{R1} + g_{R2}$, Eq. (18) reduces to

$$\mathcal{T}_{L(R)} = \frac{\Delta^2}{\Delta^2 + (g_{L1} + g_{L2})^4}, \tag{21}$$

which possesses the anti-Lorentzian line shape centered at $\Delta = 0$ with the FWHM $2(g_{L1} + g_{L2})^2$ and the minimum $\mathcal{T}_{L(R)}(\Delta = 0) = 0$, in contrast to $0 < \mathcal{T}_{L(R)} < 1$ of the BEC regime, see Fig. 2(a); however, the transmission probabilities [Eq. (20)] for $\mathrm{mod}(\tilde{\phi}_{12}, 2\pi) = \pi$ are constant unity (i.e., $\mathcal{T}_{L(R)} \equiv 1$) regardless of the specific value of the detuning Δ, exhibiting the same feature as in the BEC regime.

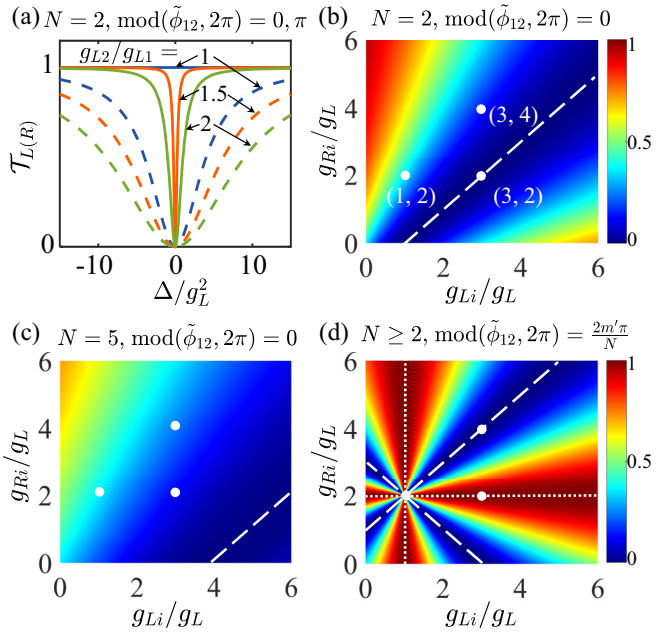

FIG. 2. Transmission probabilities $\mathcal{T}_{L(R)}$ in the Markovian regime with chiral coupling. (a) $\mathcal{T}_{L(R)}$ given by Eqs. (21) and (22) as functions of Δ by considering $g_{L2}/g_{L1} = \{1, 1.5, 2\}$ with $N = 2$ coupling points. The dashed lines correspond to the single-photon transmission spectrum under the condition of $g_{L1} + g_{L2} = g_{R1} + g_{R2}$ and mod$(\tilde{\phi}_{12}, 2\pi) = 0$, and the solid lines correspond to $|g_{L1} - g_{L2}| = |g_{R1} - g_{R2}|$ and mod$(\tilde{\phi}_{12}, 2\pi) = \pi$. For mod$(\tilde{\phi}_{12}, 2\pi) = \pi$, $\mathcal{T}_{L(R)}$ remains unity under the even coupling condition $g_{L1} = g_{L2}$, while for $g_{L1} \neq g_{L2}$, $\mathcal{T}_{L(R)}$ possesses the anti-Lorentzian lineshape of the width $2(g_{L1} - g_{L2})^2$ and undergoes a sudden jump from unity to zero at resonance $\Delta = 0$. (b)–(d) $\mathcal{T}_{L(R)}$ versus the coupling strengths g_{Li}/g_L and g_{Ri}/g_L at the ith coupling point with (b) $N = 2$, mod$(\tilde{\phi}_{12}, 2\pi) = 0$, $\Delta = \Delta_{ls} = 0$, (c) $N = 5$, mod$(\tilde{\phi}_{12}, 2\pi) = 0$, $\Delta = \Delta_{ls} = 0$, and (d) $N \geqslant 2$, mod$(\tilde{\phi}_{12}, 2\pi) = 2m'\pi/N$, $\Delta = \Delta_{ls}$, respectively. Here, we consider the N coupling points are equally spaced and set $(g_{Lj}, g_{Rj})/g_L = (1, 2)$ for $j \neq i$. The white dotted lines indicate $\mathcal{T}_{L(R)} = 1$ under the condition of $g_{Li} = g_L$ or $g_{Ri} = g_R$, i.e., the UUEC regime. The white dashed lines indicate $\mathcal{T}_{L(R)} = 0$ under the condition of $\Gamma_L = \Gamma_R$ corresponding to the BUEC regime, except the intersection (BEC) point of the lines. The white dots in (b)–(d) indicate the set of coupling strengths $(g_{Li}, g_{Ri})/g_L = \{(1, 2), (3, 2), (3, 4)\}$, with respect to the BEC, UUEC, and BUEC regimes discussed later in Fig. 3.

In the BUEC regime, the overall profile of $\mathcal{T}_{L(R)}(\Delta)$ for mod$(\tilde{\phi}_{12}, 2\pi) = 0$ is below unity and $\mathcal{T}_{L(R)}(\Delta = 0) = 0$ again for $g_{L1} + g_{L2} = g_{R1} + g_{R2}$; while for mod$(\tilde{\phi}_{12}, 2\pi) = \pi$, it is remarkable that, under the condition of $|g_{L1} - g_{L2}| = |g_{R1} - g_{R2}|$ (corresponding to $\Gamma_L = \Gamma_R \neq 0$), $\mathcal{T}_{L(R)}(\Delta)$ [Eq. (20)] reduces to

$$\mathcal{T}_{L(R)} = \frac{\Delta^2}{\Delta^2 + (g_{L1} - g_{L2})^4}, \tag{22}$$

which has the minimum $\mathcal{T}_{L(R)}(\Delta = 0) = 0$ at resonance and possesses the FWHM $2(g_{L1} - g_{L2})^2$ that can be infinitely narrow for $g_{L2}/g_{L1} \to 1$, in contrast to $\mathcal{T}_{L(R)}(\Delta) \equiv 1$ for both the BEC and the UUEC regime. In other words, an incident photon can be totally reflected or fully transmitted for the "destructive" interference phases mod$(\tilde{\phi}_{12}, 2\pi) = \pi$ when the chirality of couplings is tuned between the BEC (UUEC) regime and the BUEC regime, and moreover, the width of the reflection window can be flexibly controlled [as shown in Fig. 2(a)]. The chiral setups thus have the merits of flexibility and tunability in controlling photon transmission, offering the potential application for sensing and optical switch [2,56,58].

For $N > 2$, we consider the simplified model where the coupling strengths at the ith coupling point g_{Li} (g_{Ri}) for the left-propagating (right-propagating) photons are uniquely different from those [assumed to be identical to g_L (g_R)] of other $(N - 1)$ coupling points. Note that, in this case, both the Lamb shift Δ_{ls} and the decay rates (Γ_L, Γ_R) strongly depend on the differences of the coupling strengths $(g_L - g_{Li})$ and $(g_R - g_{Ri})$, and moreover relate to the specific position z_i of the coupling point with distinct coupling strengths, see Appendix B.

(1) For mod$(\tilde{\phi}_{12}, 2\pi) = 0$, the Lamb shifts vanish again, but the decay rates become dependent on the number of the coupling points, see Appendix B. Then, the incident photon is totally reflected at $\Delta = 0$ if the chirality of the coupling strengths satisfies

$$(N - 1)g_L + g_{Li} = (N - 1)g_R + g_{Ri}, \tag{23}$$

which reduces to $g_L + g_{Li} = g_R + g_{Ri}$ for $N = 2$. In Fig. 2(b) [Fig. 2(c)], we show $\mathcal{T}_{L(R)}[\Delta = 0, \text{mod}(\tilde{\phi}_{12}, 2\pi) = 0]$ as functions of g_{Li} and g_{Ri} (in units of g_L) with $g_R/g_L = 2$ and $N = 2$ ($N = 5$), and indicate $\mathcal{T}_{L(R)} = 0$ (or $\mathcal{R}_{L(R)} = 1$) corresponding to the condition [Eq. (23)] by the white dashed lines. Around the resonance, $\mathcal{T}_{L(R)}(\Delta)$ under the condition of Eq. (23) possess the anti-Lorentzian line shape with the FWHM $2[(N - 1)g_L + g_{Li}]^2$ scaling as N^2.

(2) For mod$(\tilde{\phi}_{12}, 2\pi) = 2m'\pi/N$, it is interesting to see that $\Gamma_L \pm \Gamma_R$ are independent of N and are simply determined by the differences of the coupling strengths $(g_L - g_{Li})$ and $(g_R - g_{Ri})$, see Appendix B. As a result, the scattering behavior is similar to the case of $N = 2$, where an incident photon is perfectly transmitted [$\mathcal{T}_{L(R)}(\Delta) \equiv 1$] if $g_L = g_{Li}$ or $g_R = g_{Ri}$, regardless of the specific value of the detuning Δ. In the BUEC regime, when the coupling strengths of the ith coupling point fulfill the condition

$$|g_L - g_{Li}| = |g_R - g_{Ri}|, \tag{24}$$

the transmission probabilities reduce to

$$\mathcal{T}_{L(R)} = \frac{(\Delta - \Delta_{ls})^2}{(\Delta - \Delta_{ls})^2 + (g_L - g_{Li})^4}, \tag{25}$$

which again possess the anti-Lorentzian line shape of the tunable width $2(g_L - g_{Li})^2$ but with the center ($\mathcal{T}_{L(R)} = 0$) shifted to $\Delta = \Delta_{ls}$. In Fig. 2(d), we show the density plot of $\mathcal{T}_{L(R)}(\Delta = \Delta_{ls})$ as functions of the chiral coupling $(g_{Lj}, g_{Rj})/g_L$, and indicate the UUEC regime by horizontal and vertical dotted lines and the BUEC regime (with $|g_L - g_{Li}| = |g_R - g_{Ri}|$) by the white dashed line. The intersection of the white dashed line with the coordinate $(g_{Lj}, g_{Rj})/g_L = (1, 2)$ corresponds to the BEC regime with $\mathcal{T}_{L(R)} = 1$. Furthermore, if we take $i = N$, i.e., the coupling strengths of the leftmost (or rightmost) coupling point are different from those of the others, the Lamb shift then reduces to $\Delta_{ls} = \frac{N}{2}(g_L^2 + g_R^2)\cot(m'\pi/N)$ (with $m' = 1, 2, \ldots, N - 1$), which

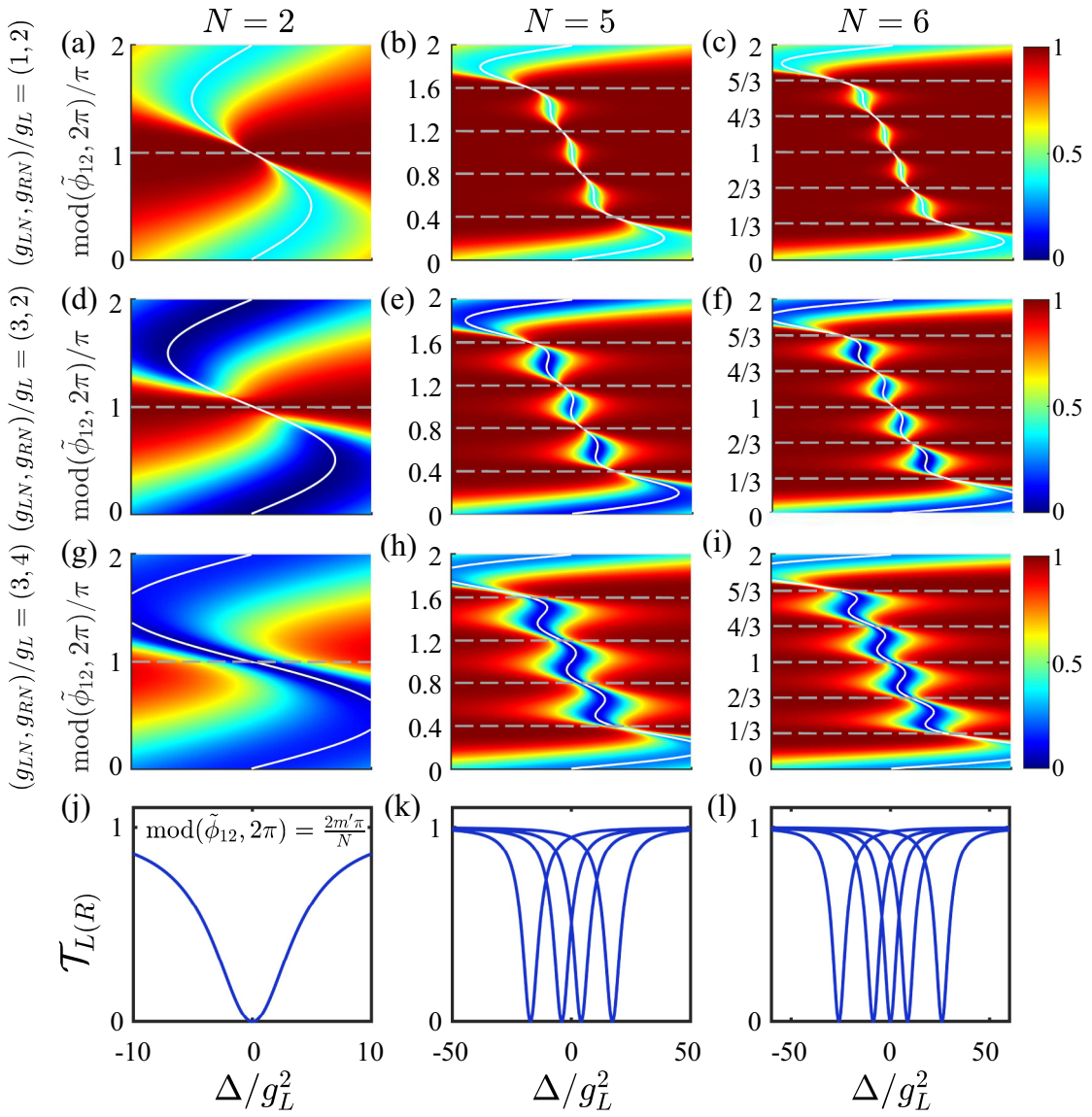

FIG. 3. Transmission probabilities $\mathcal{T}_{L(R)}$ versus Δ and $\mathrm{mod}(\tilde{\phi}_{12}, 2\pi)$ for $N = 2$, 5, 6, respectively. We consider the rightmost (i.e., Nth) coupling point which has the coupling strength $(g_{LN}, g_{RN})/g_L$ different to those of the others with $(g_{Lj}, g_{Rj})/g_L = (1, 2)$ $(j \neq N)$. As indicated in Figs. 2(b)–2(d), we set $(g_{LN}, g_{RN})/g_L = \{(1, 2), (3, 2), (3, 4)\}$, which (from top to bottom) correspond to the BEC [(a)–(c)], the UUEC [(d)–(f)], and the BUEC [(g)–(i)] regime, respectively. The white solid lines are used to label the solutions for $\Delta = \Delta_{ls}(\tilde{\phi}_{12})$, and the horizontal gray dashed lines label the phases $\mathrm{mod}(\tilde{\phi}_{12}, 2\pi) = 2m'\pi/N$ $(m' = 1, 2, \ldots, N-1)$. Panels (j)–(l) depict transmission spectrum in the BUEC regime by fixing $\mathrm{mod}(\tilde{\phi}_{12}, 2\pi) = 2m'\pi/N$, where for N being an even number, one can observe $\mathcal{T}_{L(R)} = 0$ at the resonance $\Delta = 0$ with $N - 2$ dips symmetrically around it. This can potentially be used for multichannel photon routing.

is exactly the same to that of the BEC regime, see Eq. (16). Note that Δ_{ls} is now *independent* of the coupling strengths $\{g_{LN}, g_{RN}\}$ at the Nth coupling point. Therefore, by engineering the coupling strengths $\{g_{LN}, g_{RN}\}$, the transmission probabilities $\mathcal{T}_{L(R)}(\Delta)$ can be tuned between zero and unity at the frequency detunings $\Delta = \Delta_{ls}(\tilde{\phi}_{12})$, and the width of the $(N-1)$ total reflection windows given by $2(g_L - g_{LN})^2$ can be flexibly controlled in the BUEC regime. This remarkable feature is not present in the nonchiral setup with a large N [56], as well as in a chiral setup (with only two coupling points) working in the BEC (or UUEC) regime [50,53,55].

In Fig. 3, we plot the transmission probabilities $\mathcal{T}_{L(R)}$ as functions of the detuning Δ and the two-point phase delay $\tilde{\phi}_{12}$ modulo 2π [i.e., $\mathrm{mod}(\tilde{\phi}_{12}, 2\pi)$] with $g_R/g_L = 2$ and $N = \{2, 5, 6\}$. We consider the set of coupling strengths $(g_{LN}, g_{RN})/g_L = \{(1, 2), (3, 2), (3, 4)\}$ for the Nth coupling point, corresponding to the BEC, the UUEC, and the BUEC regime, respectively. In all subfigures, the white solid lines indicate $\Delta = \Delta_{ls}(\tilde{\phi}_{12})$. We first look at the case of $N = 2$ coupling points, for $\mathrm{mod}(\tilde{\phi}_{12}, 2\pi) = 0$, the incident photon is partially reflected (i.e., $0 < \mathcal{T}_{L(R)} < 1$) in the BEC regime with $(g_{LN}, g_{RN})/g_L = (1, 2)$ [Fig. 3(a)], and nevertheless is totally reflected (i.e., $\mathcal{T}_{L(R)} = 0$) in the UUEC regime with $(g_{LN}, g_{RN})/g_L = (3, 2)$ satisfying $g_L + g_{Li} = g_R + g_{Ri}$ [Fig. 3(d)]. In both cases, the incident photon is completely transmitted for $\mathrm{mod}(\tilde{\phi}_{12}, 2\pi) = \pi$, which is indicated

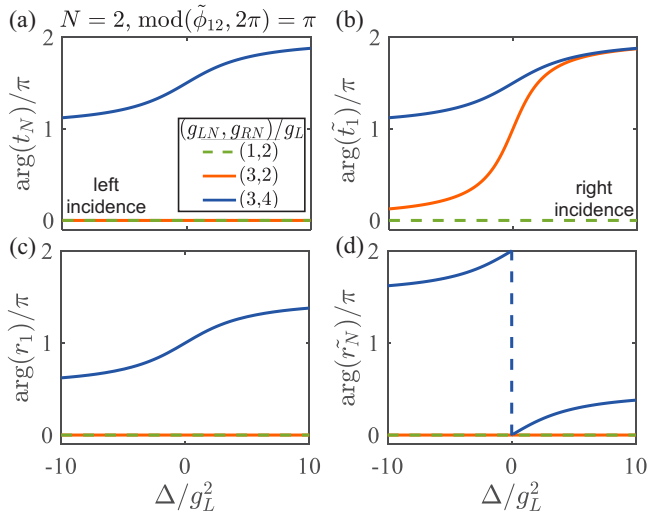

FIG. 4. Phases of the transmission $(t_N, \tilde{t}_1)$ and reflection $(r_1, \tilde{r}_N)$ coefficients versus Δ with $N = 2$. The set of coupling strengths for the second coupling point are $(g_{L2}, g_{R2})/g_L = \{(1, 2), (3, 2), (3, 4)\}$, and $(g_{L1}, g_{R1})/g_L = (1, 2)$. The two-point propagating phase is set to $\mathrm{mod}(\tilde{\phi}_{12}, 2\pi) = \pi$.

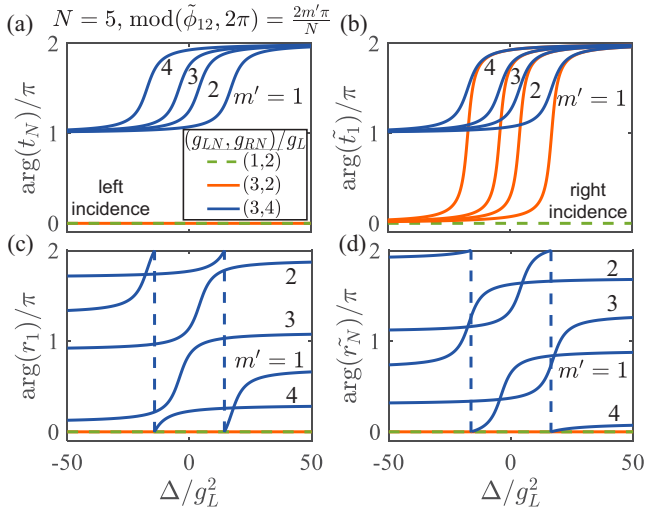

FIG. 5. Phases of the transmission $(t_N, \tilde{t}_1)$ and reflection $(r_1, \tilde{r}_N)$ coefficients versus Δ with $N = 5$. We consider the rightmost (i.e., Nth) coupling point which has the coupling strengths $(g_{LN}, g_{RN})/g_L = \{(1, 2), (3, 2), (3, 4)\}$ differing from those $(g_{LN}, g_{RN})/g_L = (1, 2)$ $(j \neq N)$] of the other coupling points. Here, the two-point propagating phases are $\mathrm{mod}(\tilde{\phi}_{12}, 2\pi) = 2m'\pi/N (m' = 1, 2, \ldots, N-1)$.

by the gray dashed line. As a result, the two red regions (corresponding to high transmission probabilities) connect to each other around $\Delta = 0$. In contrast, in the BUEC regime with $(g_{LN}, g_{RN})/g_L = (3, 4)$ (satisfying $|g_L - g_{LN}| = |g_R - g_{RN}|$), the transmission probabilities have the minimum $\mathcal{T}_{L(R)} = 0$ precisely at $\Delta = 0$ with $\mathrm{mod}(\tilde{\phi}_{12}, 2\pi) = \pi$, the two red regions are then disconnected [see Fig. 3(g)]. For $N = 5$ $(N = 6)$, as shown by the Figs. 3(b), 3(c), 3(e), and 3(f), one then finds that the incident photon is completely transmitted along the dashed lines [corresponding to $\mathrm{mod}(\tilde{\phi}_{12}, 2\pi) = 2m'\pi/N (m' = 1, 2, \ldots, N-1)$] in the BEC and the UUEC regime, and meanwhile is totally reflected at the detunings $\Delta \sim \Delta_{ls} = \frac{N}{2}(g_L^2 + g_R^2)\cot(\frac{m'\pi}{N})$ in the BUEC regime [see Figs. 3(h) and 3(i)]. Moreover, in Figs. 3(j)–3(l), we show the transmission spectrum corresponding to the cut of the plots [Figs. 3(g)–3(i)] at $\mathrm{mod}(\tilde{\phi}_{12}, 2\pi) = 2m'\pi/N$ (indicated by the dashed lines), which possess the anti-Lorentzian lineshape centered at $\Delta = \Delta_{ls}$ with a tunable width. It is worth noting that Δ_{ls} is independent of the specific values of the coupling strengths (g_{Li}, g_{Ri}) for $i = N$, thus, by setting $\Delta = \Delta_{ls}(\tilde{\phi}_{12} = \frac{2m'\pi}{N})$, the setup can potentially act as a multichannel photon router, with the frequencies of incident photons $\omega_e + \Delta_{ls}(\tilde{\phi}_{12})$ and the number of channels $N - 1$ under the condition of $\mathrm{mod}(\tilde{\phi}_{12}, 2\pi) \in (0, 2\pi)$.

Moreover, as shown in Figs. 4 and 5, we examine the phases of the transmission coefficients [$\arg(t_N)$ and $\arg(\tilde{t}_1)$] and the reflection coefficients [$\arg(r_1)$ and $\arg(\tilde{r}_N)$] for the BEC, UUEC, and BUEC regimes, respectively. The two-point propagating phases are set to $\mathrm{mod}(\tilde{\phi}_{12}, 2\pi) = 2m'\pi/N (m' = 1, 2, \ldots, N-1)$ (corresponding to the horizontal dashed lines in Fig. 3), where the incident photon can be completely transmitted or totally reflected.

For $N = 2$ and $(g_{LN}, g_{RN})/g_L = \{(1, 2), (3, 2)\}$, we find that $t_N = 1$ and $r_1 = 0$ at any Δ for a left-incident photon, leading to $\arg(t_N) = \arg(r_1) = 0$, see Figs. 4(a) and 4(c). For $(g_{LN}, g_{RN})/g_L = (3, 4)$, we alternatively have $t_N = \frac{\Delta}{\Delta + i2\Gamma_L}$ with $\arg(t_N) = -\mathrm{atan}(2\Gamma_L/\Delta)$ and $r_1 = \frac{-i\Gamma_{LR}}{\Delta + i2\Gamma_L}$ with $\arg(r_1) = \mathrm{atan}(\Delta/2\Gamma_L)$. In particular, for $\Delta \to 0$, the photon is totally reflected and the reflection coefficient r_1 picks up a phase of π. For a right-incident photon, $\arg(\tilde{t}_1)$ for $(g_{LN}, g_{RN})/g_L = (1, 2)$ and $(g_{LN}, g_{RN})/g_L = (3, 4)$ are the same as those [i.e., $\arg(t_N)$] in the left-incident case [see Figs. 4(a) and 4(b)]; but for $(g_{LN}, g_{RN})/g_L = (3, 2)$, one has $\tilde{t}_1 = \frac{\Delta - i\Gamma_L}{\Delta + i\Gamma_L}$ and $\arg(\tilde{t}_1) = -2\mathrm{atan}(\Gamma_L/\Delta)$, which now depends on the frequency detuning Δ. Moreover, for $(g_{LN}, g_{RN})/g_L = (3, 4)$, the phase of the reflection coefficient becomes $\arg(\tilde{r}_N) = \arg(r_1) + \pi$ [see Fig. 4(d)], which implies that the right-incident photon is reflected at $\Delta = 0$ with $\arg(\tilde{r}_N) = 2\pi$. Thus, in the UUEC regime, one finds $\mathcal{T}_{L(R)} = 1$ at any Δ, but a different transmission phase for the forward- and backward-propagating photons. In the BUEC regime, one obtains $\mathcal{R}_{L(R)} = 1$ at $\Delta = 0$, but a different reflection phase for the forward- and backward-propagating photons.

For $N = 5$ and $\mathrm{mod}(\tilde{\phi}_{12}, 2\pi) = 2m'\pi/N (m' = 1, 2, \ldots, N-1)$, the phases of the transmission and reflection coefficients show similar features for the forward- and the backward-propagating photons as those for $N = 2$, but now become dependent on $\tilde{\phi}_{12}$. For $(g_{LN}, g_{RN})/g_L = (3, 2)$, the transmission phases are $\arg(t_N) = 0$ and $\arg(\tilde{t}_1) = -2\mathrm{atan}[\Gamma_L/(\Delta - \Delta_{ls})]$; while for $(g_{LN}, g_{RN})/g_L = (3, 4)$, the transmission phases are $\arg(t_N) = \arg(\tilde{t}_1) = -\mathrm{atan}[2\Gamma_L/(\Delta - \Delta_{ls})]$. As shown in Figs. 5(a) and 5(b), when m' is varied, the curves corresponding to the transmission phases are transversely displaced by $\Delta_{ls}(\frac{2m'\pi}{N})$ in comparison with that of $N = 2$ [where $\arg(t_N) = -\mathrm{atan}(2\Gamma_L/\Delta)$]. However, the curves corresponding to the reflection phases $\arg(\tilde{r}_N)$ and $\arg(r_1)$ are displaced both transversely and longitudinally, see Figs. 5(c) and 5(d). Consequently, the giant atom imprints

direction-dependent phases on the propagating photon uniquely for the chiral setup in the UUEC and BUEC regimes.

IV. NONRECIPROCAL PHOTON SCATTERING WITH ATOMIC SPONTANEOUS EMISSION

We now take the atomic spontaneous decay into account, i.e., $\boldsymbol{\gamma \neq 0}$. Previously, we mentioned that nonreciprocal photon scattering (i.e., $\mathcal{T}_L \neq \mathcal{T}_R$) cannot occur for the giant atom with uniformly symmetric coupling. Moreover, it is remarkable that only reciprocal photon transport can be observed with $\gamma = 0$ despite the even or uneven chiral coupling. However, we will see that, by engineering the chirality of the coupling strengths, nonreciprocal photon transfer can be realized due to the joint effect of the chirality (i.e., $\Gamma_L \neq \Gamma_R$) and the atomic spontaneous decay $\gamma \neq 0$, and while the reflections are reciprocal $\mathcal{R}_L = \mathcal{R}_R$, see Eqs. (3) and (4). In other words, the atomic spontaneous decay of the giant atom due to its coupling to the thermal environment and the external decay due to the interfaced waveguide can cooperatively lead to nonreciprocal photon transport.

As an example, for $\gamma = \Gamma_L - \Gamma_R$ and $\Delta = \Delta_{ls}$, a photon incident from the left will be partially transmitted with the probability

$$\mathcal{T}_L = \left(1 - \frac{\Gamma_R}{\Gamma_L}\right)^2, \tag{26}$$

while a photon incident from the right will be completely isolated, i.e., $\mathcal{T}_R = 0$. For a generic situation, the nonreciprocity in transmission can be described by a contrast ratio defined as

$$I = \left|\frac{\mathcal{T}_L - \mathcal{T}_R}{\mathcal{T}_L + \mathcal{T}_R}\right| = \frac{2\gamma|\Gamma_L - \Gamma_R|}{(\Delta - \Delta_{ls})^2 + \gamma^2 + (\Gamma_L - \Gamma_R)^2}. \tag{27}$$

Thus, the nonreciprocity can only be observed when both the conditions $\gamma \neq 0$ and $\Gamma_L \neq \Gamma_R$ are simultaneously satisfied. By setting $\Delta = \Delta_{ls}$, one achieves the optimal nonreciprocity $I = 1$ with $\gamma = |\Gamma_L - \Gamma_R|$, where the spontaneous decay rate γ cancels out the difference between the effective decay rates in the forward and backward directions. For $\Delta \neq \Delta_{ls}$, the contrast ratio is always less than 1. Note that here the nonreciprocity is induced by the chirality of couplings, in contrast to that induced by non-Markovian retardation effects [53] and by synthetic gauge fields [55].

In Figs. 6(a) and 6(d), we plot the contrast ratio I as functions of the coupling strengths $(g_{Li}, g_{Ri})/g_L$ for $g_R/g_L = 2$, $\gamma/g_L^2 = 0.2$, Figs. 6(a)–6(c) $N = 5$, and Figs. 6(d)–6(f) $N \geqslant 2$. Correspondingly, we show the forward (backward) transmission probabilities $\mathcal{T}_L(\Delta = \Delta_{ls})$ [$\mathcal{T}_R(\Delta = \Delta_{ls})$] for a left-incident (right-incident) photon in Fig. 6(b) [Fig. 6(c)] with $\mathrm{mod}(\tilde{\phi}_{12}, 2\pi) = 0$ and Fig. 6(e) [Fig. 6(f)] with $\mathrm{mod}(\tilde{\phi}_{12}, 2\pi) = 2m'\pi/N$. As discussed above, the optimal nonreciprocity ($I = 1$) condition for $\mathrm{mod}(\tilde{\phi}_{12}, 2\pi) = 0$ is

$$\gamma = \pm\frac{[(N-1)g_L + g_{Li}]^2 - [(N-1)g_R + g_{Ri}]^2}{2}, \tag{28}$$

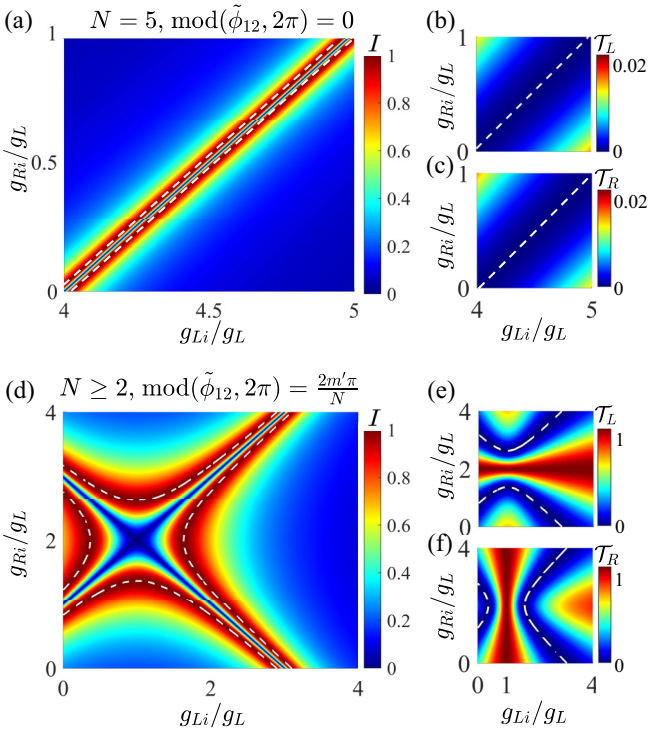

FIG. 6. Nonreciprocal transport of a single photon by including the spontaneous emission decay $\gamma/g_L^2 = 0.2$. The contrast ratio I versus g_{Li}/g_L and g_{Ri}/g_L for (a) $N = 5$, $\mathrm{mod}(\tilde{\phi}_{12}, 2\pi) = 0$ and (d) $N \geqslant 2$, $\mathrm{mod}(\tilde{\phi}_{12}, 2\pi) = 2m'\pi/N$, with the corresponding transmission probability $\mathcal{T}_L(\mathcal{T}_R)$ for a left-incident (right-incident) photon being shown in (b) [(c)] and (e) [(f)]. The white dashed lines in panels (a), (d) indicate the optimal nonreciprocity condition with $I = 1$. The white hyperbola dashed lines in (b) [(c)] and (e) [(f)] are used to label the transmission probabilities with $\mathcal{T}_{L(R)} = 0$, corresponding to $\gamma + \Gamma_L = \Gamma_R$ or $\gamma + \Gamma_R = \Gamma_L$. Other parameters are the same as in Figs. 2(c) and 2(d).

and alternatively for $\mathrm{mod}(\tilde{\phi}_{12}, 2\pi) = 2m'\pi/N$ $(m' = 1, 2, \ldots, N-1)$ is

$$\gamma = \pm\frac{(g_{Li} - g_L)^2 - (g_{Ri} - g_R)^2}{2}, \tag{29}$$

corresponding to the hyperbola branches indicated by the white dashed lines in Figs. 6(a) and 6(d). Note that for $\mathrm{mod}(\tilde{\phi}_{12}, 2\pi) = 0$, one can only observe the tail of hyperbola branches since we consider the coupling strengths being positive values; when physical parameters (coupling strengths) are extended to the complex plane, the full hyperbola branches will be clearly seen in the lower left quadrant. However, the optimal nonreciprocity is achieved at the expense of low transmission probabilities $\mathcal{T}_{L(R)}$ [shown in Figs. 6(b) and 6(c)]. For $\mathrm{mod}(\tilde{\phi}_{12}, 2\pi) = 2m'\pi/N$, we previously showed in the UUEC regime $\mathcal{T}_L = \mathcal{T}_R \equiv 1$ along $g_{Ri}/g_R = 1$ $(g_{Li}/g_L = 1)$ for $\gamma = 0$, in contrast to that, when $\gamma \neq 0$, there emerges an avoided crossing at the BEC point $(g_{Li}, g_{Ri})/g_L = (1, 2)$ with a gap $\sim 2\sqrt{2\gamma}$ of the coupling strength g_{Ri}/g_R (g_{Li}/g_L) for $\mathcal{T}_L$ $(\mathcal{T}_R)$ in Fig. 6(e) [Fig. 6(f)]. Here, the optimal nonreciprocity [Eq. (29)] corresponds to the total reflection of the incident photon $\mathcal{T}_L = 0$ or $\mathcal{T}_R = 0$, as indicated by the white dashed lines in Figs. 6(e) and 6(f). In particular, by considering the

UUEC regime (i.e., $\Gamma_L = 0$ or $\Gamma_R = 0$), we obtain the pefect nonreciprocity $I = 1$ with $\mathcal{T}_L = 0$ ($\mathcal{T}_R = 1$) or $\mathcal{T}_L = 1$ ($\mathcal{T}_R = 0$) for a left-incident (right-incident) photon since the chiral coupling g_{Ri} (g_{Li}) at the ith coupling point is counteracted by the spontaneous decay according to $g_{Ri} = g_R \pm \sqrt{2\gamma}$ ($g_{Li} = g_L \pm \sqrt{2\gamma}$). Extending to a generic case of chiral coupling, including the BEC, the UUEC, and the BUEC regime, one finally observes $I = 1$ on the hyperbola branches in Fig. 6(d). This gives a more complete picture of the chiral coupling induced nonreciprocity, which is not limited to the special cases with two-point asymmetric couplings [50,53,55].

V. NON-MARKOVIAN REGIME

So far, we consider only the Markovian regime, namely, the time for light to travel between the leftmost and the rightmost coupling points is much less than the characteristic relaxation time $\tau_{1N} \ll \tilde{\Gamma}^{-1}$. For the giant atom with N equally spaced coupling points, where $\tilde{\Gamma}$ is on the same order of $N^2 g_L^2$ (with regard to the uniformly symmetric coupling) [34,56,70], the system in the non-Markovian regime implies $\tau_{1N} = (N-1)\tau_{12}$ being comparable to or even larger than $\tilde{\Gamma}^{-1}$. Moreover, by considering the bandwidth of the order $|\Delta| \sim \tilde{\Gamma}$ or $|\Delta|/g_L^2 \sim N^2$, the effect of $\Delta\tau_{12}$ on the propagating phase $\phi_{12} = \Delta\tau_{12} + \tilde{\phi}_{12}$ (and therefore the non-Markovian retardation effect) cannot be ignored [50,53].

In Fig. 7, we show transmission spectra for $N = 2$ coupling points as functions of Δ/g_L^2 for $g_L^2\tau_{12} = 0.25, 1, 2.5$, respectively. We consider the set of coupling strengths with $(g_{L1}, g_{R1}, g_{L2}, g_{R2})/g_L = (1, 0.5, 1, 0.5)$, $(g_{L1}, g_{R1}, g_{L2}, g_{R2})/g_L = (1, 0.5, 1, 1.5)$, and $(g_{L1}, g_{R1}, g_{L2}, g_{R2})/g_L = (1, 0.5, 0.5, 1)$, according to the specific chiral conditions Eqs. (23) and (24). For $g_L^2\tau_{12} = 0.25$, the weak non-Markovian effect starts to influence the transmission spectra. As shown in Fig. 7(a), for $\mathrm{mod}(\tilde{\phi}_{12}, 2\pi) = 0$, all of the scattering spectrum have a single minimum at $\Delta = 0$, but with a different width when the coupling strengths $(g_{L2}, g_{R2})/g_L$ are varied. For $\mathrm{mod}(\tilde{\phi}_{12}, 2\pi) = \pi$, as $|\Delta|/g_L^2$ increases, the transmission probabilities in the UUEC [with $(g_{L1}, g_{R1}, g_{L2}, g_{R2})/g_L = (1, 0.5, 1, 1.5)$] and the BEC [with $(g_{L1}, g_{R1}, g_{L2}, g_{R2})/g_L = (1, 0.5, 1, 0.5)$] regime decline weakly from $\mathcal{T}_{L(R)}(\Delta = 0) = 1$, while in the BUEC regime [with $(g_{L1}, g_{R1}, g_{L2}, g_{R2})/g_L = (1, 0.5, 0.5, 1)$], $\mathcal{T}_{L(R)}(\Delta)$ quickly transits from zero to almost one for being out of resonance [see Fig. 7(b)]. For $g_L^2\tau_{12} = 1$, the system enters the intermediate non-Markovian regime. For $\mathrm{mod}(\tilde{\phi}_{12}, 2\pi) = 0$, there emerges a wide frequency interval where $\mathcal{T}_{L(R)}$ remain approximately unchanged, see Fig. 7(c). In particular, $\mathcal{T}_{L(R)} \simeq 0$ in the frequency interval for $(g_{L2}, g_{R2})/g_L = (0.5, 1)$ (corresponding to the BUEC regime), which is referred to as a photonic band gap with the bandwidth scaling as $|\Delta|/g_L^2 \propto N^2$ [56]. Note that this feature was previously found in a nonchiral setup [56], but with a large number of coupling points. For $\mathrm{mod}(\tilde{\phi}_{12}, 2\pi) = \pi$, as shown in Fig. 7(d), $\mathcal{T}_{L(R)}(\Delta)$ starts to oscillate and additional minima at around $\Delta/g_L^2 \sim 3$ can be found. In the deep non-Markovian regime with $g_L^2\tau_{12} = 2.5$ [as shown in Figs. 7(e) and 7(f)], the flat lineshape in the band gap splits and exhibits side valleys

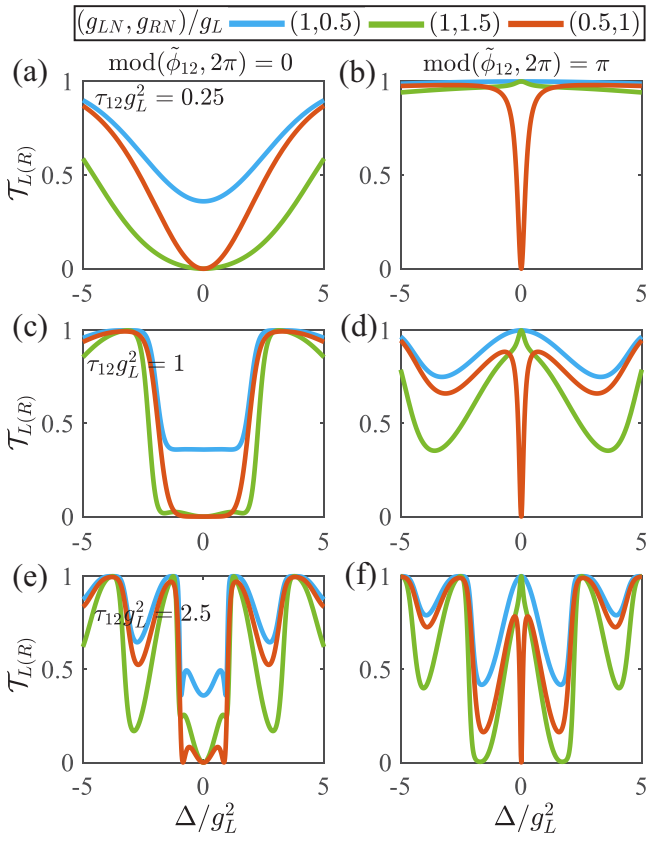

FIG. 7. Transmission spectra in the non-Markovian regime with $N = 2$ and $\gamma = 0$, where (a), (c), (e) $\mathrm{mod}(\tilde{\phi}_{12}, 2\pi) = 0$ (the left panels), and (b), (d), (f) $\mathrm{mod}(\tilde{\phi}_{12}, 2\pi) = \pi$ (the right panels). The photon propagation time is set as $g_L^2\tau_{12} = \{0.25, 1, 2.5\}$, corresponding to the weak, intermediate, and deep non-Markovian regimes, respectively. Coupling strengths for the two coupling points are $(g_{L1}, g_{R1}, g_{L2}, g_{R2})/g_L = \{(1, 0.5, 1, 0.5), (1, 0.5, 1, 1.5), (1, 0.5, 0.5, 1)\}$, which correspond to the BEC (blue), the UUEC (green), and the BUEC (red) regimes, respectively.

near $\Delta = 0$ for $\mathrm{mod}(\tilde{\phi}_{12}, 2\pi) = 0$, and only in the case of $(g_{L2}, g_{R2})/g_L = (0.5, 1)$ with respect to the BUEC regime, we observe $\mathcal{T}_{L(R)} = 0$ at the two side valleys; in addition, for $(g_{L2}, g_{R2})/g_L = (1, 1.5)$ and $(g_{L2}, g_{R2})/g_L = (1, 0.5)$, $\mathcal{T}_{L(R)}(\Delta)$ oscillate between 0 and 1 as $|\Delta|$ increases whether $\mathrm{mod}(\tilde{\phi}_{12}, 2\pi) = 0$ or $\mathrm{mod}(\tilde{\phi}_{12}, 2\pi) = \pi$.

In Fig. 8, we show the transmission spectra as functions of Δ/g_L^2 with $N = 5$ for $g_L^2\tau_{12} = 0.01, 0.04$, and 0.1, which correspond to the weak, intermediate, and deep non-Markovian regimes, respectively. We consider the propagating time $\tau_{1N} \sim (N^2 g_L^2)^{-1}$ from the first to the last coupling point, and the frequency bandwidth is set to $|\Delta| \sim N^2 g_L^2$. Furthermore, we assume that the set of coupling strengths for the Nth coupling point are $(g_{LN}, g_{RN})/g_L = \{(1, 0.6), (1, 2.6), (0, 1.6)\}$, and the coupling strengths for the other coupling points are $(g_{Lj}, g_{Rj})/g_L = (1, 0.6)$, corresponding to the three chiral coupling regimes discussed above. Note that the coupling strengths $(g_{LN}, g_{RN})/g_L = (0, 1.6)$ satisfy both the conditions $g_{LN} - g_{RN} = (1-N)(g_L - g_R)$ and $|g_{LN} - g_L| = |g_R - g_{RN}|$, while the coupling strengths $(g_{LN}, g_{RN})/g_L = (1, 2.6)$ satisfy

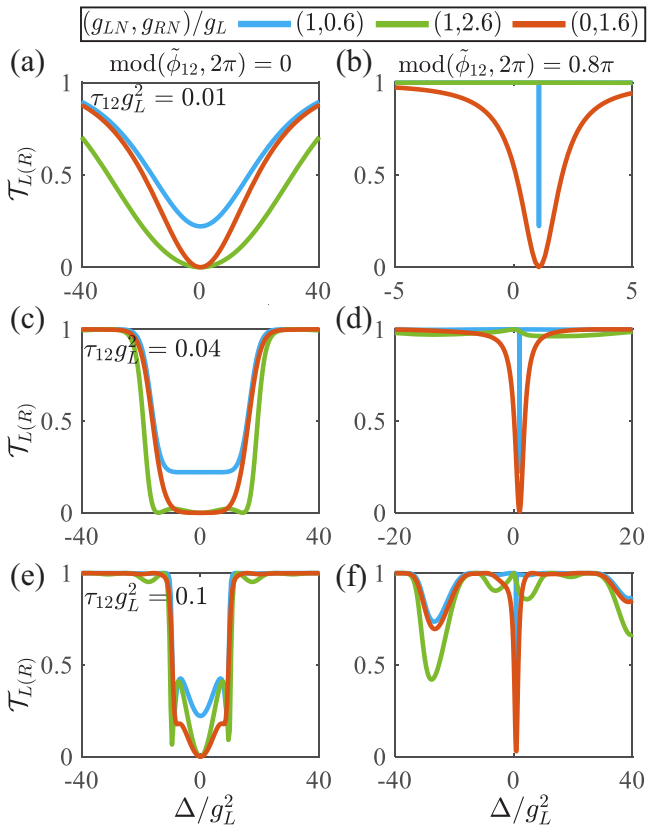

FIG. 8. Transmission spectrum in the non-Markovian regime with $N = 5$ and $\gamma = 0$, where (a), (c), (e) $\mathrm{mod}(\tilde{\phi}_{12}, 2\pi) = 0$, and (b), (d), (f) $\mathrm{mod}(\tilde{\phi}_{12}, 2\pi) = 0.8\pi$ [i.e., $\mathrm{mod}(\tilde{\phi}_{12}, 2\pi) = 2m'\pi/N$ with $m' = 2$ without loss of generality]. We set the coupling strengths of the Nth coupling point as $(g_{LN}, g_{RN})/g_L = \{(1, 0.6), (1, 2.6), (0, 1.6)\}$ and that of the others as $(g_{Lj}, g_{Rj})/g_L = (1, 0.6)$ $(j \neq N)$, which correspond to the BEC (blue), the UUEC (green), and the BUEC (red) regime, respectively. Moreover, the photon propagation time is set as $g_L^2\tau_{12} = \{0.01, 0.04, 0.1\}$, corresponding to the weak, intermediate, and deep non-Markovian regimes, respectively.

$g_{LN} - g_{RN} = (1 - N)(g_L - g_R)$ only. For $\mathrm{mod}(\tilde{\phi}_{12}, 2\pi) = 0$, as shown by Figs. 8(a), 8(c), and 8(e), the transmission spectra with $g_L^2\tau_{12} = \{0.01, 0.04, 0.1\}$ show oscillation behaviors similar to those of $N = 2$ in the same non-Markovian regime, and as $|\Delta|$ increases, $\mathcal{T}_{L(R)}(\Delta)$ saturate to unity after a few oscillations in the intermediate and deep non-Markovian regimes. For $\mathrm{mod}(\tilde{\phi}_{12}, 2\pi) = 2m'\pi/N$, the lineshape of the scattering spectra becomes asymmetric for an odd number of coupling points, see Figs. 8(b), 8(d), and 8(f), where we take $m' = 2$ [i.e., $\mathrm{mod}(\tilde{\phi}_{12}, 2\pi) = 0.8\pi$] as an example. In particular, since the Lamb shift Δ_{ls} is nonvanishing for $\mathrm{mod}(\tilde{\phi}_{12}, 2\pi) = 2m'\pi/N$, the time delay $\sim\Delta\tau_{12}$ will lead to a shift of the dip [corresponding to $\mathcal{T}_{L(R)}(\Delta_{ls}) \to 0$] for the BUEC regime [i.e., $(g_{LN}, g_{RN})/g_L = (0, 1.6)$], while in comparison, $\mathcal{T}_{L(R)}$ remain unity at resonance [i.e., $\mathcal{T}_{L(R)}(\Delta = 0) \equiv 1$] for the UUEC $[(g_{LN}, g_{RN})/g_L = (1, 2.6)]$ and BEC $[(g_{LN}, g_{RN})/g_L = (1, 0.6)]$ regimes. Note that, since there may not exist an appropriate detuning Δ fulfilling both $\Gamma_L = \Gamma_R$ and $\Delta = \Delta_{ls}$, $\mathcal{T}_{L(R)}$ in the BEC regime suffer from a sudden jump to $\mathcal{T}_{L(R)}(\Delta_{ls}) = [(\Gamma_L - \Gamma_R)/(\Gamma_L + \Gamma_R)]^2$ at the detuning $\Delta = \Delta_{ls}$ [see the blue curve in Figs. 8(b), 8(d), and 8(f)], which does not occur in the case of $N = 2$. In general, for $\mathrm{mod}(\tilde{\phi}_{12}, 2\pi) = 2m'\pi/N$, the oscillation amplitudes of $\mathcal{T}_{L(R)}(\Delta)$ become larger when the system enters the intermediate and deep non-Markovian regimes.

VI. EXPERIMENTAL FEASIBILITY AND CONCLUSION

The giant atom model under consideration can be found in Refs. [39,40], where the three- and six-coupling-point architectures are realized with nonchiral waveguides and are used to demonstrate decoherence-free interaction [39] or electromagnetically induced transparency [40]. In these experiments, a frequency-tunable transmon qubit capacitively couples to a meandering microwave TL at multiple points, where the number of coupling points is limited by the device geometry and the physical size of the transmon qubit. The qubit can be regarded as a two-level system when the atom-waveguide coupling strength $\sim g_L$ (of a few MHz) is much smaller than the level anharmonicity (with the maximum value a few hundred MHz) [62], and the atomic decay rate is on the order of $\sim$0.1 MHz [39]. Moreover, the capacitive coupling at each connection point can be tuned by mediating the qubit-field interaction with superconducting quantum interference devices (SQUIDs) and tuning the magnetic fluxes threading them [40]. For the two-point propagating phase $\phi_{12} = \omega_e|z_2 - z_1|/v$ around the qubit frequency ω_e, where v is the speed of light in the waveguide, a phase ϕ_{12} of 2π corresponds to a two-point distance $|z_2 - z_1| = 2\pi v/\omega_e \sim 20$ mm, which can be controlled with great precision [40]. However, chiral quantum optics with photonic reservoir was studied with many architectures [71], e.g., photonic-crystal waveguides or optical nanofibers with transversely confined light [32,72], and microwave TLs with circulators [64–67]. Considering that the giant artificial atoms demonstrated in Refs. [39,40] are based on coupling to the microwave TLs, the scattering phenomena unique to giant atoms chirally coupled with waveguides may be demonstrated by using microwave circulators to provide the chirality [49,64–67]. Although the non-Markovian effect has not yet been observed in the microwave-photons-based systems so far, it can be alternatively demonstrated with the SAW-based systems [35], or by increasing the atom-waveguide coupling with a well-designed superconducting flux qubit [73].

In conclusion, we study the photon scattering spectra by a giant atom, which is chirally coupled to a waveguide at multiple equally spaced points. The chirality is categorized in terms of the evenness of coupling strengths in the left and right propagation directions, and is divided into three regimes, i.e., the BEC, UUEC, and BUEC regimes. In the Markovian limit and for the two-point propagating phase being $\mathrm{mod}(\tilde{\phi}_{12}, 2\pi) = 0$, the incident photon can be totally reflected at resonance and the transmission spectra possess the anti-Lorentzian line shape with the width depending on the number of coupling points N. For the two-point propagating phase satisfying $\mathrm{mod}(\tilde{\phi}_{12}, 2\pi) = 2m'\pi/N$, the incident photon is fully transmitted at $\Delta = \Delta_{ls}$ in the BEC and the UUEC regimes, but can be totally reflected in the BUEC regime, where, interestingly, the transmission probabilities can be flexibly

tuned at $(N-1)$ fixed frequencies by engineering the chirality of couplings, allowing for multiple-channel photon routing; moreover, the giant-atom-waveguide coupling can imprint direction-dependent phases on the scattering coefficients. Due to the chiral coupling, the maximum nonreciprocity in photon scattering (corresponding to the contrast ratio of unity) can be achieved when the atomic spontaneous decay is taken into account, differing from the non-Markovianity induced effect in other chiral waveguide QED systems [50,53]. The non-Markovian retardation effect manifested by the scattering spectra reflects itself mainly in the photonic band gap and the oscillatory behavior between total reflection and full transmission, especially in the intermediate and deep non-Markovian regimes, respectively. The giant-atom-waveguide system with chiral coupling thus offers flexible ways for single-photon routing.

ACKNOWLEDGMENTS

H.W. acknowledges support from the National Natural Science Foundation of China (NSFC) under Grants No. 11774058 and No. 12174058. Y.L. acknowledges support from the NSFC under Grants No. 12074030 and No. 12274107.

APPENDIX A: SOLUTION OF TRANSMISSION AND REFLECTION COEFFICIENTS

Inserting Eqs. (1) and (2) into the stationary Schrödinger equation $H|\psi\rangle = E|\psi\rangle$, we find that the probability amplitudes obey the following relations:

$$\begin{aligned}
Ec_{gL}(z) &= \left(\omega_0 + iv_g\frac{\partial}{\partial z}\right)c_{gL}(z) \\
&\quad + \sum_{j=1}^{N}\delta(z-z_j)\sqrt{v_g}g_{Lj}e^{ik_0 z}c_{e0}, \\
Ec_{gR}(z) &= \left(\omega_0 - iv_g\frac{\partial}{\partial z}\right)c_{gR}(z) \\
&\quad + \sum_{j=1}^{N}\delta(z-z_j)\sqrt{v_g}g_{Rj}e^{-ik_0 z}c_{e0}, \\
(\Delta+i\gamma)c_{e0} &= \int dz\sum_{j=1}^{N}\delta(z-z_j)\sqrt{v_g}[g_{Lj}e^{-ik_0 z}c_{gL}(z) \\
&\quad + g_{Rj}e^{ik_0 z}c_{gR}(z)],
\end{aligned} \tag{A1}$$

where $\Delta = \omega(k) - \omega_e$ is the detuning between the incident photons and the atomic transition $|g\rangle \leftrightarrow |e\rangle$. Now suppose a photon is incident from the left port and the atom is initially in $|g\rangle$, the probability amplitudes, due to the δ-function potential effect of the atom at the coupling point can be formed as

$$\begin{aligned}
c_{gR}(z) &= e^{i(k-k_0)z}\Bigg[\Theta(z_1-z) + \sum_{j=1}^{N-1}t_j\Theta(z-z_j)\Theta(z_{j+1}-z) \\
&\quad + t_N\Theta(z-z_N)\Bigg],
\end{aligned}$$

$$\begin{aligned}
c_{gL}(z) &= e^{-i(k-k_0)z}\Bigg[r_1\Theta(z_1-z) \\
&\quad + \sum_{j=2}^{N}r_j\Theta(z-z_{j-1})\Theta(z_j-z)\Bigg],
\end{aligned} \tag{A2}$$

where t_j (r_j) is the transmission (reflection) coefficient for the jth coupling point, t_N (r_1) is the transmission (reflection) coefficient for the last (first) coupling point, and $\Theta(z-z_j)$ is the Heaviside step function. While for the right-incident case, the probability amplitudes alternatively take the form

$$c_{gR}(z) = e^{i(k-k_0)z}\left[\sum_{j=1}^{N-1}\tilde{r}_j\Theta(z-z_j)\Theta(z_{j+1}-z) + \tilde{r}_N\Theta(z-z_N)\right],$$

$$\begin{aligned}
c_{gL}(z) &= e^{-i(k-k_0)z}\Bigg[\tilde{t}_1\Theta(z_1-z) + \sum_{j=2}^{N}\tilde{t}_j\Theta(z-z_{j-1})\Theta(z_j-z) \\
&\quad + \Theta(z-z_N)\Bigg],
\end{aligned} \tag{A3}$$

with $\tilde{t}_j$, $\tilde{r}_j$ being the corresponding transmission and reflection coefficients as in the right-incident case. Substituting Eqs. (A2) and (A3) into Eq. (A1), one readily obtains the transmission and reflection coefficients (t_N and r_1) for a left-incident photon and the transmission and reflection coefficients ($\tilde{t}_1$ and $\tilde{r}_N$) for a right-incident photon. Furthermore, the transmission and reflection probabilities are given by $\mathcal{T}_L = |t_N|^2$ ($\mathcal{T}_R = |\tilde{t}_1|^2$) and $\mathcal{R}_L = |r_1|^2$ ($\mathcal{R}_R = |\tilde{r}_N|^2$) for a left-incident (right-incident) photon, respectively.

APPENDIX B: LAMB SHIFT AND EFFECTIVE DECAY RATES FOR THE UUEC AND BUEC REGIMES

For $N > 2$, we consider the simplified model where the coupling strengths at the ith coupling point g_{Li} (g_{Ri}) for the left-propagating (right-propagating) photons are uniquely different from that [assumed to be identical to g_L (g_R)] of all the other $(N-1)$ coupling points. A brief calculation shows that the Lamb shift is given by

$$\begin{aligned}
\Delta_{ls} &= \frac{g_L^2+g_R^2}{2}(NS_1 - S_N) - \frac{g_L(g_L-g_{Li}) + g_R(g_R-g_{Ri})}{2} \\
&\quad \times (2S_1 + S_{i-1} - S_i + S_{N-i} - S_{N-i+1}),
\end{aligned} \tag{B1}$$

with $S_j(\tilde{\phi}_{12}) = \sin(j\tilde{\phi}_{12})/(1-\cos\tilde{\phi}_{12})$, $j \in \mathbf{N}$, and the effective decay rates are

$$\begin{aligned}
\Gamma_L \pm \Gamma_R &= \frac{g_L^2 \pm g_R^2}{2}C_N + \frac{(g_L-g_{Li})^2 \pm (g_R-g_{Ri})^2}{2} \\
&\quad + \frac{g_L(g_L-g_{Li}) \pm g_R(g_R-g_{Ri})}{2} \\
&\quad \times (C_{i-1} - C_i + C_{N-i} - C_{N-i+1}),
\end{aligned} \tag{B2}$$

with $C_j(\tilde{\phi}_{12}) = \sin^2(\frac{1}{2}j\tilde{\phi}_{12})/\sin^2(\frac{1}{2}\tilde{\phi}_{12})$. (1) The Lamb shifts vanish for $\mathrm{mod}(\tilde{\phi}_{12}, 2\pi) = 0$ due to $S_j(\tilde{\phi}_{12}) = 0$, but the decay rates in Eq. (B2) become dependent on the number of the

coupling points according to

$$\Gamma_L \pm \Gamma_R = \frac{[(N-1)g_L + g_{Li}]^2 \pm [(N-1)g_R + g_{Ri}]^2}{2}. \tag{B3}$$

It follows that the transmission probabilities are

$$\mathcal{T}_{L(R)} = \frac{4\Delta^2 + \{[(N-1)g_L + g_{Li}]^2 - [(N-1)g_R + g_{Ri}]^2\}^2}{4\Delta^2 + \{[(N-1)g_L + g_{Li}]^2 + [(N-1)g_R + g_{Ri}]^2\}^2}. \tag{B4}$$

(2) For $\mathrm{mod}(\tilde{\phi}_{12}, 2\pi) = 2m'\pi/N$, there exist the mathematical identities $C_j(\tilde{\phi}_{12}) = C_{N-j}(\tilde{\phi}_{12})$ and $S_j(\tilde{\phi}_{12}) = -S_{N-j}(\tilde{\phi}_{12})$ $(j = 0, 1, \ldots, N)$, from which we readily find the Lamb shifts being nonvanishing and N-dependent

$$\Delta_{ls} = NS_1 \frac{g_L^2 + g_R^2}{2} - (S_1 + S_{i-1} - S_i) \times [g_L(g_L - g_{Li}) + g_R(g_R - g_{Ri})], \tag{B5}$$

and more interestingly, the *N-independent* effective decay rates

$$\Gamma_L \pm \Gamma_R = \tfrac{1}{2}[(g_L - g_{Li})^2 \pm (g_R - g_{Ri})^2]. \tag{B6}$$

[1] D. Roy, C. M. Wilson, and O. Firstenberg, Rev. Mod. Phys. **89**, 021001 (2017).

[2] X. Gu, A. F. Kockum, A. Miranowicz, Y.-x. Liu, and F. Nori, Phys. Rep. **718-719**, 1 (2017).

[3] A. S. Sheremet, M. I. Petrov, I. V. Iorsh, A. V. Poshakinskiy, and A. N. Poddubny, Rev. Mod. Phys. **95**, 015002 (2023).

[4] P. Lodahl, S. Mahmoodian, and S. Stobbe, Rev. Mod. Phys. **87**, 347 (2015).

[5] R. Uppu, L. Midolo, X. Zhou, J. Carolan, and P. Lodahl, Nat. Nanotechnol. **16**, 1308 (2021).

[6] R. J. Coles, D. M. Price, J. E. Dixon, B. Royall, E. Clarke, P. Kok, M. S. Skolnick, A. M. Fox, and M. N. Makhonin, Nat. Commun. **7**, 11183 (2016).

[7] M. Jalali Mehrabad, A. P. Foster, R. Dost, E. Clarke, P. K. Patil, A. M. Fox, M. S. Skolnick, and L. R. Wilson, Optica **7**, 1690 (2020).

[8] A. Sipahigil, R. E. Evans, D. D. Sukachev, M. J. Burek, J. Borregaard, M. K. Bhaskar, C. T. Nguyen, J. L. Pacheco, H. A. Atikian, C. Meuwly, R. M. Camacho, F. Jelezko, E. Bielejec, H. Park, M. Lončar, and M. D. Lukin, Science **354**, 847 (2016).

[9] J. Arjona Martínez, R. A. Parker, K. C. Chen, C. M. Purser, L. Li, C. P. Michaels, A. M. Stramma, R. Debroux, I. B. Harris, M. Hayhurst Appel, E. C. Nichols, M. E. Trusheim, D. A. Gangloff, D. Englund, and M. Atatüre, Phys. Rev. Lett. **129**, 173603 (2022).

[10] M. Pasini, N. Codreanu, T. Turan, A. R. Moral, C. F. Primavera, L. De Santis, H. K. Beukers, J. M. Brevoord, C. Waas, J. Borregaard, and R. Hanson, arXiv:2311.12927.

[11] M. Pompili, S. L. N. Hermans, S. Baier, H. K. C. Beukers, P. C. Humphreys, R. N. Schouten, R. F. L. Vermeulen, M. J. Tiggelman, L. dos Santos Martins, B. Dirkse, S. Wehner, and R. Hanson, Science **372**, 259 (2021).

[12] A. Blais, A. L. Grimsmo, S. M. Girvin, and A. Wallraff, Rev. Mod. Phys. **93**, 025005 (2021).

[13] C. Toninelli, I. Gerhardt, A. S. Clark, A. Reserbat-Plantey, S. Götzinger, Z. Ristanović, M. Colautti, P. Lombardi, K. D. Major, I. Deperasińska, W. H. Pernice, F. H. L. Koppens, B. Kozankiewicz, A. Gourdon, V. Sandoghdar, and M. Orrit, Nat. Mater. **20**, 1615 (2021).

[14] E. Vetsch, D. Reitz, G. Sagué, R. Schmidt, S. T. Dawkins, and A. Rauschenbeutel, Phys. Rev. Lett. **104**, 203603 (2010).

[15] N. V. Corzo, B. Gouraud, A. Chandra, A. Goban, A. S. Sheremet, D. V. Kupriyanov, and J. Laurat, Phys. Rev. Lett. **117**, 133603 (2016).

[16] H. L. Sørensen, J.-B. Béguin, K. W. Kluge, I. Iakoupov, A. S. Sørensen, J. H. Müller, E. S. Polzik, and J. Appel, Phys. Rev. Lett. **117**, 133604 (2016).

[17] A. Goban, C.-L. Hung, S.-P. Yu, J. D. Hood, J. A. Muniz, J. H. Lee, M. J. Martin, A. C. McClung, K. S. Choi, D. E. Chang, O. Painter, and H. J. Kimble, Nat. Commun. **5**, 3808 (2014).

[18] A. Goban, C.-L. Hung, J. D. Hood, S.-P. Yu, J. A. Muniz, O. Painter, and H. J. Kimble, Phys. Rev. Lett. **115**, 063601 (2015).

[19] C.-H. Yan and L.-F. Wei, Opt. Express **23**, 10374 (2015).

[20] O. Astafiev, A. M. Zagoskin, A. A. Abdumalikov, Jr., Y. A. Pashkin, T. Yamamoto, K. Inomata, Y. Nakamura, and J. S. Tsai, Science **327**, 840 (2010).

[21] I.-C. Hoi, T. Palomaki, J. Lindkvist, G. Johansson, P. Delsing, and C. M. Wilson, Phys. Rev. Lett. **108**, 263601 (2012).

[22] I.-C. Hoi, C. Wilson, G. Johansson, J. Lindkvist, B. Peropadre, T. Palomaki, and P. Delsing, New J. Phys. **15**, 025011 (2013).

[23] A. F. van Loo, A. Fedorov, K. Lalumière, B. C. Sanders, A. Blais, and A. Wallraff, Science **342**, 1494 (2013).

[24] Y. Liu and A. A. Houck, Nat. Phys. **13**, 48 (2017).

[25] H. J. Kimble, Nature (London) **453**, 1023 (2008).

[26] L.-M. Duan and C. Monroe, Rev. Mod. Phys. **82**, 1209 (2010).

[27] S. Wehner, D. Elkouss, and R. Hanson, Science **362**, eaam9288 (2018).

[28] M. Bello, G. Platero, J. I. Cirac, and A. González-Tudela, Sci. Adv. **5**, eaaw0297 (2019).

[29] X. Wang, T. Liu, A. F. Kockum, H.-R. Li, and F. Nori, Phys. Rev. Lett. **126**, 043602 (2021).

[30] S. Mahmoodian, G. Calajó, D. E. Chang, K. Hammerer, and A. S. Sørensen, Phys. Rev. X **10**, 031011 (2020).

[31] A. Frisk Kockum, in *International Symposium on Mathematics, Quantum Theory, and Cryptography*, edited by T. Takagi, M. Wakayama, K. Tanaka, N. Kunihiro, K. Kimoto, and Y. Ikematsu (Springer, Singapore, 2021), pp. 125–146.

[32] M. V. Gustafsson, T. Aref, A. F. Kockum, M. K. Ekström, G. Johansson, and P. Delsing, Science **346**, 207 (2014).

[33] R. Manenti, A. F. Kockum, A. Patterson, T. Behrle, J. Rahamim, G. Tancredi, F. Nori, and P. J. Leek, Nat. Commun. **8**, 975 (2017).

[34] L. Guo, A. Grimsmo, A. F. Kockum, M. Pletyukhov, and G. Johansson, Phys. Rev. A **95**, 053821 (2017).

[35] G. Andersson, B. Suri, L. Guo, T. Aref, and P. Delsing, Nat. Phys. **15**, 1123 (2019).

[36] G. Andersson, M. K. Ekström, and P. Delsing, Phys. Rev. Lett. **124**, 240402 (2020).

[37] Z.-Q. Wang, Y.-P. Wang, J. Yao, R.-C. Shen, W.-J. Wu, J. Qian, J. Li, S.-Y. Zhu, and J. Q. You, Nat. Commun. **13**, 7580 (2022).
[38] A. Frisk Kockum, P. Delsing, and G. Johansson, Phys. Rev. A **90**, 013837 (2014).
[39] B. Kannan, M. J. Ruckriegel, D. L. Campbell, A. Frisk Kockum, J. Braumüller, D. K. Kim, M. Kjaergaard, P. Krantz, A. Melville, B. M. Niedzielski, A. Vepsäläinen, R. Winik, J. L. Yoder, F. Nori, T. P. Orlando, S. Gustavsson, and W. D. Oliver, Nature (London) **583**, 775 (2020).
[40] A. M. Vadiraj, A. Ask, T. G. McConkey, I. Nsanzineza, C. W. Sandbo Chang, A. F. Kockum, and C. M. Wilson, Phys. Rev. A **103**, 023710 (2021).
[41] Q.-Y. Qiu, Y. Wu, and X.-Y. Lü, Sci. China Phys. Mech. Astron. **66**, 224212 (2023).
[42] A. F. Kockum, G. Johansson, and F. Nori, Phys. Rev. Lett. **120**, 140404 (2018).
[43] A. Carollo, D. Cilluffo, and F. Ciccarello, Phys. Rev. Res. **2**, 043184 (2020).
[44] L. Du, L. Guo, and Y. Li, Phys. Rev. A **107**, 023705 (2023).
[45] L. Du, L. Guo, Y. Zhang, and A. F. Kockum, Phys. Rev. Res. **5**, L042040 (2023).
[46] S. Guo, Y. Wang, T. Purdy, and J. Taylor, Phys. Rev. A **102**, 033706 (2020).
[47] D. Cilluffo, A. Carollo, S. Lorenzo, J. A. Gross, G. M. Palma, and F. Ciccarello, Phys. Rev. Res. **2**, 043070 (2020).
[48] K. H. Lim, W.-K. Mok, and L.-C. Kwek, Phys. Rev. A **107**, 023716 (2023).
[49] A. Soro and A. F. Kockum, Phys. Rev. A **105**, 023712 (2022).
[50] L. Du, Y.-T. Chen, and Y. Li, Phys. Rev. Res. **3**, 043226 (2021).
[51] L. Du, Y. Zhang, J.-H. Wu, A. F. Kockum, and Y. Li, Phys. Rev. Lett. **128**, 223602 (2022).
[52] X. Wang and H.-R. Li, Quantum Sci. Technol. **7**, 035007 (2022).
[53] J. Zhou, X.-L. Yin, and J.-Q. Liao, Phys. Rev. A **107**, 063703 (2023).
[54] L. Du and Y. Li, Phys. Rev. A **104**, 023712 (2021).
[55] Y.-T. Chen, L. Du, L. Guo, Z. Wang, Y. Zhang, Y. Li, and J.-H. Wu, Commun. Phys. **5**, 215 (2022).
[56] Q. Y. Cai and W. Z. Jia, Phys. Rev. A **104**, 033710 (2021).
[57] S. L. Feng and W. Z. Jia, Phys. Rev. A **104**, 063712 (2021).
[58] Y. P. Peng and W. Z. Jia, Phys. Rev. A **108**, 043709 (2023).
[59] W. Zhao, Y. Zhang, and Z. Wang, Front. Phys. **17**, 42506 (2022).
[60] X.-L. Yin, Y.-H. Liu, J.-F. Huang, and J.-Q. Liao, Phys. Rev. A **106**, 013715 (2022).
[61] A. Ask, Y.-L. L. Fang, and A. F. Kockum, arXiv:2011.15077.
[62] J. Koch, T. M. Yu, J. Gambetta, A. A. Houck, D. I. Schuster, J. Majer, A. Blais, M. H. Devoret, S. M. Girvin, and R. J. Schoelkopf, Phys. Rev. A **76**, 042319 (2007).
[63] C. Joshi, F. Yang, and M. Mirhosseini, Phys. Rev. X **13**, 021039 (2023).
[64] S. R. Sathyamoorthy, L. Tornberg, A. F. Kockum, B. Q. Baragiola, J. Combes, C. M. Wilson, T. M. Stace, and G. Johansson, Phys. Rev. Lett. **112**, 093601 (2014).
[65] K. M. Sliwa, M. Hatridge, A. Narla, S. Shankar, L. Frunzio, R. J. Schoelkopf, and M. H. Devoret, Phys. Rev. X **5**, 041020 (2015).
[66] B. J. Chapman, E. I. Rosenthal, J. Kerckhoff, B. A. Moores, L. R. Vale, J. A. B. Mates, G. C. Hilton, K. Lalumière, A. Blais, and K. W. Lehnert, Phys. Rev. X **7**, 041043 (2017).
[67] C. Müller, S. Guan, N. Vogt, J. H. Cole, and T. M. Stace, Phys. Rev. Lett. **120**, 213602 (2018).
[68] C. Gonzalez-Ballestero, E. Moreno, F. J. Garcia-Vidal, and A. Gonzalez-Tudela, Phys. Rev. A **94**, 063817 (2016).
[69] J.-T. Shen and S. Fan, Phys. Rev. A **79**, 023837 (2009).
[70] A. Ask, M. Ekström, P. Delsing, and G. Johansson, Phys. Rev. A **99**, 013840 (2019).
[71] P. Lodahl, S. Mahmoodian, S. Stobbe, A. Rauschenbeutel, P. Schneeweiss, J. Volz, H. Pichler, and P. Zoller, Nature (London) **541**, 473 (2017).
[72] I. Söllner, S. Mahmoodian, S. L. Hansen, L. Midolo, A. Javadi, G. Kiršanskė, T. Pregnolato, H. El-Ella, E. H. Lee, J. D. Song, S. Stobbe, and P. Lodahl, Nat. Nanotechnol. **10**, 775 (2015).
[73] P. Forn-Díaz, J. García-Ripoll, B. Peropadre, J.-L. Orgiazzi, M. Yurtalan, R. Belyansky, C. Wilson, and A. Lupascu, Nat. Phys. **13**, 39 (2017).